Numerical simulations of multiobject RBC scattering - a Bremmer series approach[⋆,⋆⋆]

B.G. Wallner[a,1,]

[a] *Mistelvaegen 13, 2441 71 Doesjebro, Sweden, +46732484998*

Abstract

In this paper we will study light propagation in whole blood with hematocrit up to $hct = 21\%$ by numerically solving Helmholtz equation. This will be done by using an iterative approach, a generalized Bremmer series to numerically simulate a plane wave propagating through a three dimensional geometrical model describing randomly distributed RBCs. The article will discuss various approaches for analyzing light propagation in whole blood and the theory section will start of from Maxwell's equations and explain the ideas behind the Bremmer series. To make comparisons possible with existing research also single RBC scattering will be analyzed as well as using non-wave approaches such as Beer-Lambert's law for intensity comparison. The article will mostly consider electromagnetics and biophysics but also connections to the key ideas behind the implemented computer program used for the simulation.

The results of the simulations show that the computer program developed shows a good agreement for a one-dimensional slab when compared with Beer-Lambert's law together with Fresnel's equations for the intensity transmission. For a $1mm$ layer consisting of blood-plasma background and $16 \cdot 7.76\mu m$ layers having refractive index of an RBC give a sub 1% agreement compared to Beer-Lambert and Fresnel. The method also produces a good result for single RBCs where the near-field shows good agreement with other studies which uses other methods for field-calculation. The method however fails to produce a consistent result for multiobject RBC scattering where the method gives a diverging intensity. The results for the multiobject case also does not improve if increasing the size of the mesh or introducing smoothing for the change in refractive index. Decreasing the contrast between electrical permitivity for RBC and background to $< 5\%$ makes the intensity not to diverge in which case the absorption will be the dominating factor.

Keywords: electromagnetics, biophysics, bremmer series, numerical simulation

⋆tbd.

⋆⋆tbd.

Email address: bogoeran.wallner@gmail.com (B.G. Wallner)

[1] Master of Science in Engineering Physics, Lund university, Faculty of Engineering.

1. Introduction

TODO: General overview of current methods for calculating scattering problem such as FTDT, T-matrix. Discussion of areas using Bremmer series.

2. Analysis

The purpose of the analysis is to gradually increase the level of complexity, starting from wellknown physics of plane waves to Maxwell's equations and then the method for solving the in-homogenous Helmholtz equation. The content will thus start from undergraduate level and procede to content considered as graduate level and then the results of this paper is more towards research. The aim is that anyone with a fair knowledge of electromagnetics, optics and mathematics shall be able to follow the paper from start to end. We will also try to connect betwen content typically teached at engineering faculty with what is teached at physics departments. The same content is often presented in different ways, in engineering there is a lot of focus at solving Maxwell's equations and the energy flux density is described by Poyntings vector while at physics departments similar problems are sometimes described in terms of irradiance, Beer-Lambert's law, Fresnels equations etc. Even though the problems are conceptually the same when e.g. describing the optics of light. In this paper we will try to connect these areas. During the analysis and the rest of the paper the cartesian coordinate z is used for the propagation direction whereas x, y is used for describing the plane in which the field oscillates. Concerning the computational model the field is discretized or sampled and each sampling- or grid-point we will hereafter refer to as a node following the terminology used in finite element method. The total number of nodes will be refered to as a mesh. Let's start by reviewing the time-harmonic plane wave.

2.1. The time-harmonic plane wave

In this first section we will start by defining the time-harmonic plane wave or equally, the monochromatic plane wave. A monochromatic wave is a wave containing one single frequency. At first, studying a monochromatic wave may seem like a theoretical construction but some waves in nature are indeed inherently monochromatic, at least to a certain degree, while others are not. However, from Fourier analysis we know that we can describe any function depending upon time by superposition of monochromatic waves with different angular frequencys which motivates the usage. In this paper we define the time-harmonic plane wave of the electric field as

$$\bar{E}(z,t) = \bar{E}_0 cos(\omega t - kz) = \bar{E}_0 Re(e^{j(\omega t - kz)}) \tag{1}$$

where z is the direction of propagation perpendicular to $\bar{E}(z,t)$, ω the angular frequency and k is the wavenumber defined as $k = \omega/c$ in free space. We

will later consider k when propagation occurs in a lossy medium where it will be a complex number. In cartesian coordinates $\bar{E} = (E_x, E_y)$ and for a linear polarized wave in x we have $E_x = E_0 Re(e^{j(\omega t - kz)})$ and $E_y = 0$. The property of the time-harmonic wave is that $\omega t - kz = constant$, as t increases z must increase and thus moves in the z direction. Extending the definition to three dimensions we can write

$$\bar{E}(\bar{r}, t) = \bar{E}_0 Re(e^{j(\omega t - \bar{k} \cdot \bar{r})}) \tag{2}$$

If for some $\bar{r}_0$ it is such that $(\bar{r} - \bar{r}_0) \cdot \bar{k} = 0$ then $\bar{r}$ and $\bar{r}_0$ defines a plane perpendicular to the propagation direction and thus $\bar{k} \cdot \bar{r} = constant$. At that plane the value of $\bar{E}(\bar{r}, t)$ is constant and as time increases consequtive planes will have values between $- \mid \bar{E}_0 \mid$ and $\mid \bar{E}_0 \mid$ and changing periodically with angular frequency ω. The choice of $cos(...)$ is a natural choice since at $t = 0$ and $z = 0$ the amplitude of the wave is $\mid \bar{E}_0 \mid$ but we could equally use $sin(...)$ and phase-shift to what would suit our needs. We also notice the use of j instead of i for the complex notation following electrical engineering tradition as well as the time convention $e^{j\omega t}$. We should also have in mind that a time-harmonic wave does not have to be a plane wave, throwing a stone in the water creates harmonic waves being cylindric and from a light-bulb or a star the light-waves are rather associated with a spherical symmetry. Although, at long distance both these examples can be approximated by a plane wave in a small enough region. At the same time, a plane wave does not need to be time-harmonic since the only requirement is that $\bar{k} \cdot \bar{r} = constant$. Further discussions concerning time-harmonic plane waves can be found in [1] [12] [20].

2.2. Maxwell's equation's

Maxwell's equations describe the relationship between the electric field $\bar{E}(\bar{r}, t)$, the magnetic field $\bar{H}(\bar{r}, t)$, the electric flux density $\bar{D}(\bar{r}, t)$, the magnetic flux density $\bar{B}(\bar{r}, t)$ and the current density $\bar{J}(\bar{r}, t)$. The equations on differential form is formulated as

$$\nabla \times \bar{E} = -\frac{\partial \bar{B}}{\partial t} \tag{3}$$

$$\nabla \times \bar{H} = \bar{J} + \frac{\partial \bar{D}}{\partial t} \tag{4}$$

$$\nabla \cdot \bar{B} = 0 \tag{5}$$

$$\nabla \cdot \bar{D} = \rho \tag{6}$$

where ρ is the charge density and the explicit dependence on $\bar{r}, t$ has been omitted. To this we also add conservation of charge

$$\nabla \cdot \bar{J} + \frac{\partial \rho}{\partial t} = 0 \tag{7}$$

which is an equation of continuity for charge. By using (1), (2) and (5) it's possible to derive (3) and (4). The connection between $\bar{D}$ and $\bar{E}$ is formulated

as $\bar{D} = \epsilon_0 \bar{E}$ in free space and in a general medium $\bar{D} = \epsilon_0 \bar{\epsilon} \bar{E}$ where ϵ_0 is the dielectric constant in vacuum and $\bar{\epsilon}$ is a unitless dielectric tensor which is dependent upon material properties. In this work the RBCs and the blood plasma is each considered isotropic and homogenous. We can write the representation of the tensor as

$$\bar{\epsilon} = \begin{pmatrix} \epsilon_{11} & \epsilon_{12} & \epsilon_{13} \\ \epsilon_{21} & \epsilon_{22} & \epsilon_{23} \\ \epsilon_{31} & \epsilon_{32} & \epsilon_{33} \end{pmatrix} = \begin{pmatrix} \epsilon_r & 0 & 0 \\ 0 & \epsilon_r & 0 \\ 0 & 0 & \epsilon_r \end{pmatrix} \tag{8}$$

where $\epsilon_r = \epsilon' - j \cdot \epsilon''$ is a complex number describing the relative permitivity. A similar analysis can be done for the magnetic field $\bar{H}(\bar{r}, t)$. In this paper we will focus on the electric field and ignore further analysis of the magnetic field unless nescessary for the context.

2.3. Helmholtz wave-equation

The Helmholtz equation is a direct consequence of Maxwell's equations for a time-harmonic field and while Helmholtz equation is found in almost every physics textbook it's not often used in engineering texts where it often is mentioned as the wave-equation for the time-harmonic case. As we have previously seen a time-harmonic field has the dependency $e^{j\omega t}$ and applying this to (3) and (4) we get

$$\nabla \times \bar{E} = -j\omega \bar{B} = -j\omega \mu_0 \bar{\mu} \bar{H} \tag{9}$$

$$\nabla \times \bar{H} = j\omega \epsilon_0 \bar{\epsilon} \bar{E} \tag{10}$$

where we have used $\bar{\mu}$ the relative permeability for the relationship between magnetic field and magnetic flux density in analogy to the permitivity and the material is considered source-free. If we take the curl of (9) we get

$$\nabla \times (\nabla \times \bar{E}) = -j\omega \nabla \bar{\times} B = -j\omega \mu_0 \bar{\mu} \nabla \times \bar{H} \tag{11}$$

But from (10) we have

$$\nabla \times (\nabla \times \bar{E}) = -j\omega \mu_0 \bar{\mu} (j\omega \epsilon_0 \bar{\epsilon} \bar{E}) = \omega^2 \mu_0 \bar{\mu} \epsilon_0 \bar{\epsilon} \bar{E} \tag{12}$$

In this paper we are dealing with an isotropic homogenous non-magnetic material and thus the diagonal elements of $\bar{\mu}$ is $\mu_r = 1$. We re-write (12) as

$$\nabla \times (\nabla \times \bar{E}) - \omega^2 \mu_0 \bar{\mu} \epsilon_0 \bar{\epsilon} \bar{E} = 0 \tag{13}$$

For a cartesian coordinate system we can use the relation $\nabla \times (\nabla \times \bar{F}) = \nabla(\nabla \cdot \bar{F}) - \nabla^2 \bar{F}$ which can be found in any book covering vector analysis or mathematics handbook [34]. Since the material is source-free we have that $\nabla \cdot \bar{D} = 0$ and thus we get

$$\nabla^2 \bar{E} + \omega^2 \mu_0 \bar{\mu} \epsilon_0 \bar{\epsilon} \bar{E} = (\nabla^2 + k^2) \bar{E} = 0 \tag{14}$$

where $k = \omega\sqrt{\mu_0\bar{\mu}\epsilon_0\bar{\epsilon}}$ is the wave-number in the medium. With the assumption of non-magnetic material and furthermore isotropic homogenous we get one scalar equation ($\bar{\epsilon}$ is diagonal) for each cartesian coordinate

$$(\nabla^2 + k^2)E_x = 0 \tag{15}$$

where $k = \omega\sqrt{\mu_0\epsilon_0\epsilon_r}$. This is the scalar Helmholtz equation. If using the free-space wave-number $k_0 = 2\pi/\lambda_0 = \omega\sqrt{\mu_0\epsilon_0}$ we can write the wave-number $k = k_0\sqrt{\epsilon_r}$ (if the material is magnetic we also add a μ_r). The expression $\sqrt{\epsilon_r}$ is the refractive index n and in a general medium k, n, ϵ_r, μ_r are complex numbers.

In previous section we specified the time-harmonic plane wave as $E_x = \bar{E}_0 Re(e^{j(\omega t - kz)}) \cdot \hat{x}$. For the Helmholtz equation the $e^{j\omega t}$ is implicit and we can write $E_x = E_{0x}e^{-jkz}$. If we assume a plane wave propagating through vacuum $k = k_0$which then reduces plane wave to $E_x = E_{0x}e^{-jk_0z}$. Applying (15) to this expression

$$(\nabla^2 + k^2)E_x = (\nabla^2 + k_0^2)E_x = \left(\frac{\partial^2}{\partial^2 z} + k_0^2\right) E_{0x}e^{-jk_0z} = (-k_0^2 + k_0^2)E_{0x} = 0 \tag{16}$$

where the Laplacian $\nabla^2 = \left(\partial^2/\partial^2 x + \partial^2/\partial^2 y + \partial^2/\partial^2 z\right)$ only contributes in z direction since the value of E_x is per definition constant in the plane xy. One can realize that also a plane wave propagatng in the negative z direction is also a solution (15) and thus a full solution is

$$E_x = E_{0x}^{+}e^{-jk_0z} + E_{0x}^{-}e^{jk_0z} \tag{17}$$

which represents two plane waves propagating in opposite direction in free-space. We can also extend the reasoning by letting k be any real number. What we have done so far is that we have assumed a solution to (15) and in (16) that it indeed is a solution. Thus, we have not solved (15) but merely showed that a time-harmonic plane wave satifies Helmholtz equation in a homogenous isotropic material. We can also make some other conclusions, if $E_0 \rightarrow E(x, y)$ our analysis would render a number of partial differential equations since the Laplacian would need to applied to this expression. The easy problem has then been transformed into a harder problem. Furthermore, if the material is in-homogenous, i.e. $k = k(x, y, z)$, the problem becomes much harder and can only be analytically solved in some special cases where a plane boundary is the first case we will study. The analysis will thus continue by letting the freely propagating plane waves interact with a plane boundary.

When solving the equation numerically for an in-homogenous problem we will get solutions for every node having the form $\bar{E}_{ph} = \bar{E}'_{ph} - j\bar{E}''_{ph}$ ("ph" as in phasor) which is a complex number. But when formulating the Helmholtz equation we have assumed a time-harmonic behaviour $e^{j\omega t}$ which is not part of the complex solution $\bar{E}_{ph}$. Thus we need to add this and the solution will then be $\bar{E} = (\bar{E}'_{ph} - j\bar{E}''_{ph}) \cdot e^{j\omega t}$. But furthermore, even though $\bar{E}$ fulfills Maxwells equations we know that the electric field must not be a complex entity, the

nature is real, and evaluating the previous expression and then taking the real-part gives us

$$\bar{E}_{phys} = \bar{E}'_{ph} cos(\omega t) + \bar{E}''_{ph} sin(\omega t) \tag{18}$$

It's important to stress that the choice of $e^{j\omega t}$ instead of $cos(\omega t)$ we only chose out of convinience, at the same time getting a non physical imaginary component. However, during the calculations the resulting imaginary parts can give us other type of useful information e.g. calculating the the complex Poynting vector.

The Poynting vector describes the energy-flux, the size and direction of the energy contained in the fields and is defined as $\bar{S}(\bar{r}, t) = \bar{E}(\bar{r}, t) \times \bar{H}(\bar{r}, t)$ which to the size is proportional to $\bar{E}(\bar{r}, t)^2$ in a non-magnetic isotropic material. If we evaluate the physical field above in some fixed direction, thus skipping the vector notation of the electric field, we get $E(\bar{r}, t)^2 = E^2_{phys} = (E'_{ph} cos(\omega t) + E''_{ph} sin(\omega t))^2 = E^2_{ph}{}' cos^2(\omega t) + E^2_{ph}{}'' sin^2(\omega t) + E'_{ph} E''_{ph} sin(2\omega t)$. If we average this expression over $\omega t = 0..2\pi$ the odd-function contribution $E'_{ph} E''_{ph} sin(2\omega t)$ will zero out while the sine- and cosine squares will become $1/2$. Thus the time-average over one period is then $S_{av} \propto 1/2(E^2_{ph}{}' + E^2_{ph}{}'')$ which actually could be written down directly by having the phasors and using $\bar{S}_{av} = 1/2 \cdot \bar{E}_{ph} \times \bar{H}^*_{ph}$. Below we will discuss the concept of intensity (irradiance) which is exactly the time-average of the Poynting vector in a given direction.

2.4. Fresnels equations

In the previous section we showed that the plane wave was a solution to Maxwell's equations for a wave travelling in a homogenous isotropic material. We concluded that if the wavenumber $k = k(x, y, z)$ was dependent upon the spatial coordinates, i.e. that the complex refractive index changed with position the problem became hard to solve unless we had special cases. The simplest special case is the plane boundary and as mentioned before we assign the boundary to the xy plane. While elementary physics is teaching us about optical rays, the Snell's law $n_i sin(\theta_i) = n_t sin(\theta_t)$ which relates how a ray is refracted in a surface between materials with different refractive indexes, the law of reflection $\theta_r = \theta_i$ teaching us that the reflected ray is reflected in a surface with the same angle as the incoming ray, it does not say anything about how much of the "ray" is reflected and how much is transmitted. To do this we need to approach the problem from an electromagnetic approach. First of all we need to define a reference which is called the plane of incidence which we define as the plane perpendicular to the xy plane, e.g. we can choose the xz plane. We have then two cases, either the electric field oscillates parallell to the xz plane and this we call p-polarization. If we instead have a wave with the electric field oscillating in the xy plane we call this s-polarization which then is perpendicular to the plane of incidence. This is called s-polarization after "senkrecht" which in german means perpendicular. So what we are trying to achieve here is a number of expressions relating the amplitude of the transmitted and reflected field to the incoming field. And to do this the boundary conditions for the electric

and magnetic field is used. For the electric field there are two conditions for a boundary, the first is that the tangential component of the electric field $\bar{E}$ shall be continous over a boundary. The second is that the normal component of the electric flux density $\bar{D} = \epsilon_0 \bar{\epsilon} \bar{E}$ shall be continous over a boundary. An excellent derivation can be studied in Hecht [12]. In our case we have a plane wave with an angle of indidence $\theta_i = 0$ which relates the reflected field and the transmitted field with the factors

$$r = \frac{n_t - n_i}{n_t + n_i} \tag{19}$$

$$t = \frac{2n_i}{n_i + n_t} \tag{20}$$

If we consider an RBC having refractive index $n'_{rbc} = 1.406$ and the blood plasma $n'_{ba} = 1.345$ we get $r = 0.022174$ and $t = 0.97783$ when the wave is reflected from background to RBC. We also need to be aware that if the wave is reflected inside the RBC we will get $r = -0.022174$ which means that the reflected wave will have the opposite polarization and will decrease the electric field.

From the Fresnel's equations we can with the knowledge of the electric field also determine the intensity of the reflected and transmitted wave, the transmittance and the reflectance we can write as

$$R = \left(\frac{n_t - n_i}{n_t + n_i} \right)^2 \tag{21}$$

$$T = \frac{4n_i n_t}{(n_i + n_t)^2} \tag{22}$$

and using refractive indexes above we get $T = 0.999508$ and $R = 0.00049168$. What is of outermost importance is to be able to understand that the total intensity needs to consider both the reflected and transmitted intensity. Let's assume the RBC to be an infinite in layer in xy with some thickness Δz. A laser beam described as a plane wave impinges at the surface having intensity I_{in} and is reflected with $I^r_{in} = R \cdot I_{in} = 0.00049168 \cdot I_{in}$. Thus, the total intensity above the surface is $I_{tot} = I_{in} - I^r_{in} = 0.999508 \cdot I_{in}$. The transmitted intensity within the RBC is $I^{rbc}_t = T \cdot I_{in} = 0.999508 \cdot I_{in}$. Within the RBC nothing happens until the lower surface of the RBC is reached and we once again get a reflection $I^{rbc}_r = R \cdot I^{rbc}_t = 0.00049143 \cdot I_{in}$. Thus, in total the intensity within the RBC is $I^{rbc}_{tot} = I^{rbc}_t - I^{rbc}_r = 0.999508 \cdot I_{in} - 0.00049143 \cdot I_{in} = 0.999017 \cdot I_{in}$. And the transmitted intensity from within the RBC is $I_t = T \cdot I^{rbc}_t = 0.999508 \cdot 0.999508 \cdot I_{in} = 0.999017 \cdot I_{in}$. Thus, by taking only one internal reflection into account we expect to get out 99.9017% of the intensity when propagating through the RBC.

Area	Transmitted intensity	Reflected intensity	Total intensity
Above RBC	I_{in}	$0.00049168 \cdot I_{in}$	$0.999508 \cdot I_{in}$
Within RBC	$0.999508 \cdot I_{in}$	$0.00049143 \cdot I_{in}$	$0.999017 \cdot I_{in}$
Below RBC	$0.999017 \cdot I_{in}$	-	$0.999017 \cdot I_{in}$

With this information it's possible to verify that the Bremmer series give us a reasonable solution.

2.5. Beer-Lambert's law and attenuation of the wave

In this section we will look at Beer-Lambert's law and derive an expression for the intenstity which can be used for comparison with the results from the numerical simulation of Helmholtz equation. Beer-Lambert's law is found in almost every basic physics textbook but following the engineering tradition with Helmholtz equation it's rarely seen in engineering texts on electromagnetics. As with Helmholtz equation the attenuation of the electric field is a direct consequence of Maxwell's equations and the formulation of Poynting's vector using a complex refractive index with a non-zero imaginary part. When solving the wave-equation we can take both the attenuation of the wave as well as the scattering into account. In this work the scattering is described by refraction and backward reflection of the wave. Beer-Lambert's law in it's original form, excluding adding of the scattering coefficient, only deals with the attenuation due to absorption and gives no information about the electromagnetic nature. The attenuation part of the wave can be described by the attenuation coefficient and we will connect this coeffiecient to the refractive index and the electrical permitivity. When discussing the wave-equation we use the electric field but traditionally Beer-Lambert's law is formulated with intensity (we will use intensity instead of irradiance). The relationship between the light-intensity and the electric field is according to $I \propto E_0^2$ for a free-space propagating wave $\bar{E} = Re\{E_0 \cdot e^{j(\omega t - \bar{k}\cdot\bar{r})}\}$ where $\bar{k}$ is the free-space wavenumber for a non-attenuated wave. Assume a one-dimensional slab in the z-direction having an attenuation coefficient $\alpha = \alpha(z)$. The attenuation coefficient is usually used with Beer-Lambert's law instead of e.g. refractive index or permitivity and the expression for the attenuation of the intensity can be written as

$$I(z) = I_0 \cdot e^{-\int_0^z \alpha(z)\cdot dz} \tag{23}$$

The attenuation coefficient is connected to the the complex refractive index $n(\omega) = n'(\omega) - j \cdot n''(\omega)$ and this relation can be formulated as

$$n''(\omega) = \frac{c \cdot \alpha(\omega)}{2 \cdot \omega} \Longrightarrow \alpha(\omega) = \frac{2 \cdot \omega \cdot n''(\omega)}{c} = \frac{4\pi \cdot n''(\omega)}{\lambda} \tag{24}$$

where $\lambda = 2\pi \cdot c/\omega$, c is the speed of light, λ the light wave-length and ω the angular frequency. For a constant attenuation coefficient we can reduce (1) to

$$I(z) = I_0 \cdot e^{-\alpha \cdot z} \tag{25}$$

and using (2) we end up with

$$I(z) = I_0 \cdot e^{-4\pi \cdot n''(\omega)\cdot z/\lambda} \tag{26}$$

Here we have used the complex part of the refractive index and for the sake of clarity consider formulating the attenuated electric field as $\bar{E}(z,t) =$

$e^{-\alpha \cdot z/2} Re\{E_0 \cdot e^{j(\omega t - kz)}\}$ for a wave travelling in the z-direction where k is the wavenumber for a non-attenuated wave. The wave is attenuated with the attenuation coefficient $\alpha/2$. This implies that the intensity $I \propto \mid e^{-\alpha \cdot z/2} Re\{E_0 \cdot e^{j(\omega t - kz)}\} \mid^2 = \mid E_0 \mid^2 \cdot e^{-\alpha \cdot z}$ which is (3). In some texts the attenuation factor of the intensity is described as $e^{-2\alpha \cdot z}$ when defining α (not $\alpha/2$!) as the attenuation of the field and not the intensity. But we can also write the electric field, now taking the attenuation into account in the expression for the field, by using the complex refractive index as $\bar{E}(z,t) = Re\{E_0 \cdot e^{j(\omega t - n(\omega) \cdot \omega \cdot z/c)}\} = Re\{E_0 \cdot e^{j\omega(t - n(\omega) \cdot z/c)}\}$. By using $n = n' - j \cdot n''$ we get $I \propto \mid Re\{E_0 \cdot e^{j(\omega t - kz)}\} \mid^2 = \mid E_0 \mid^2 \cdot e^{-2\omega \cdot n''(\omega) \cdot z/c}$. Thus $\mid E_0 \mid^2 \cdot e^{-\alpha \cdot z} = \mid E_0 \mid^2 \cdot e^{-2\omega \cdot n''(\omega) \cdot z/c}$ and we can see that (2) must be fullfilled.

When dealing with electromagnetic waves the permitivity is mostly used instead of the refractive index and the relationship between these is as follows. Let $n = n' - j \cdot n''$ and $\epsilon_r = \epsilon' - j \cdot \epsilon''$ where $\epsilon_r = \epsilon_{complex}/\epsilon_0$ is the relative permitivity. Then $\epsilon_r = n^2 = (n'^2 - n''^2) - 2 \cdot j \cdot n' \cdot n''$ and thus $\epsilon' = (n'^2 - n''^2)$ and $\epsilon'' = 2 \cdot n' \cdot n''$ (extinction coefficient) where we have followed the sign convention of $e^{j\omega t}$ (if using "physics notation" $e^{-i\omega t}$ we would use $n = n' + i \cdot n''$ by $j \to -i$). Let's next be more specific about our setup.

We have so far briefly discussed Beer-Lambert's law and attenuation in general terms. Our intention has been to be able to use the expression (4) to be able to compare with the results from the simulation of Helmholtz equation and we will start with an approach and only consider the absorption. This will later be modified by instead considering both absorption and scattering cross-section, essentially by adding a scattering coefficient. However, as we have previously seen the permitivity is not constant in our model and thus we can't use (4) directly. Consider the setup in Figure 1.

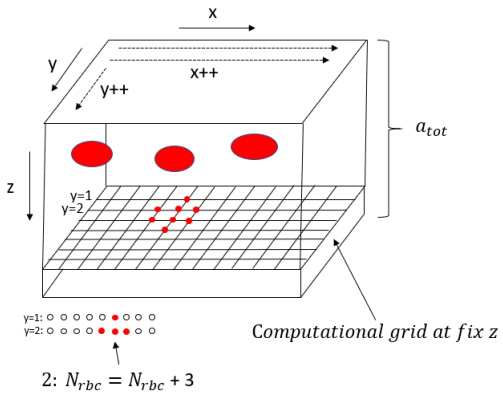

Figure 1: An overview of the three-dimensional model where the RBCs are distributed in a quadratic mesh. The red dots represent a node being part of an RBC. By calculating the number of nodes being within an RBC as well as the total number of nodes we get the volume ratio of RBCs.

Our idea is the following (we will interchangeably use refractive index and

permitivity without any notice). Both the RBCs and the surrounding background is individually isotropic and homogenous (and for the problem locally non-dispersive). Furthermore, the imaginary part of the background permitivity $\epsilon''_{ba} = 0$. The numerical simulation for solving Helmholtz equation give the possibility to determine the hematocrit H, i.e. the volume-fraction of RBCs $V_{rbc}/V_{tot} = N_{rbc}/N_{tot}$. Here N_{rbc} is the number of nodes belonging to an RBC and N_{tot} is the total number of nodes. To be able to get a number for comparing the intensities we first tranform the three-dimensional problem containing an inhomogeneous medium to a one-dimensional problem containing one part having refractive index n''_{rbc} and one part having n''_{ba} (now only dealing with imaginary parts). See Figure 2.

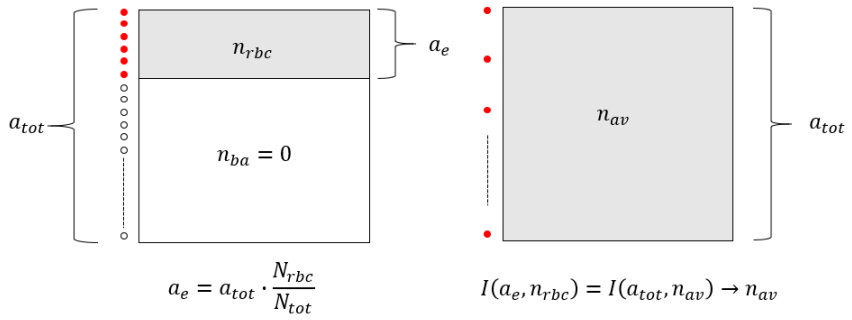

Figure 2: When having calculated the number of nodes belonging to RBCs we can calculate an effective refractive index. We can think of it as the nodes belonging to RBCs are being "smeared out".

This give us, which we might have guessed, the following $n''_{av} = n''_{rbc} \cdot (a_e/a_{tot}) = n''_{rbc} \cdot (N_{rbc}/N_{tot}) = n''_{rbc} \cdot H$ where H is the hematocrit (volume fraction of RBCs). Using this in (4) we finally get an expression

$$I(z) = I_0 \cdot e^{-4\pi \cdot n''_{rbc} H \cdot z/\lambda} = I_0 \cdot e^{-\alpha \cdot H \cdot z} \tag{27}$$

where n''_{rbc} is the imaginary part of the complex refractive index. What we now have achieved is that by simple reasoning we can conclude that the only thing when going from the inhomogenous problem to a corresponding homogenous problem is that we need to scale according to the hematocrit level. Thus, we have reduced a complex problem to a scalar multiplication. However, it assumes that we can calculate the hematocrit H.

As mentioned the model above only takes absorption into account but as we know we also need to account for scattering. This has been investigated in a number of studies and in this paper we reference Bosschaart [2] where values for absorption and scattering coefficient has been compiled from several other articles as well as theoretically calculated. Instead of our α above the article uses an effective attenuation coefficient $\mu_{eff} = \sqrt{3\mu_{abs}(\mu_{abs} + \mu'_s)}$ where in our case $\alpha = \mu_{abs} = \mu_a$. The μ'_s is the reduced scattering coefficient which

can be calculated as $\mu_s' = \mu_s(1-g)$ where g is the scattering anisotropy. The article present tabulated values per wavelength for μ_a, μ_s, g which makes it possible to calculate the effective attenuation coefficient. However, these values are tabulated for $HCT = 45\%$ and to be able compare with our setup we need to scale the value according to $H/45\%$ where we measure H in %. Thus, we then get

$$I(z) = I_0 \cdot e^{-\mu_{eff} \cdot H \cdot z/45\%} \tag{28}$$

For $\lambda = 635nm$ the following values are tabulated and used in this article, $\mu_a = 0.24mm^{-1}$, $\mu_s = 88.63mm^{-1}$ and $g = 0.9827$. This give $\mu_{eff} = 1.1299mm^{-1}$. In the simulation we will be able to achieve $H = 21\%$ and using this in (28) for a $1mm$ layer of blood give us $I(z = 1mm)/I_0 = 59\%$. Also, we can now calculate that for the RBC using (24) $\epsilon_{rbc}'' = 2 \cdot n' \cdot n'' = 2{\cdot}1.406{\cdot}\mu_a{\cdot}\lambda/4\pi = 2{\cdot}1.406{\cdot}0.24{\cdot}632.8{\cdot}10^{-6}/4\pi = 3.3985{\cdot}10^{-5}$. For the real parts $\epsilon_{rbc}' \simeq n_{rbc}^2 = 1.406^2 = 1.977$ and for the background $\epsilon_{ba}' \simeq n_{ba}^2 = 1.345^2 = 1.809$ And this level is enough for our purpose, for more details see [2].

2.6. The Bremmer series

TODO: Explain at essentially the level of Ishimaru to see the transition from layers to WKB and then Bremmer series.

2.6.1. The one-dimenational slab

To be able to verify the results from the implementation of the Bremmer series a geometrical model describing a one-dimensional slab is used. Or rather, since the model is three-dimensional, a quadratic section in xy plane and elongated into z direction. This is done since it's easy to calculate theoretically with Beer-Lambert's law and Fresnel's equations according to the previous discussion. The model contain 16 sections, each $7.76\mu m$ of thickness having the refractive index $n_{rbc}' = 1.406$. As we have discussed previously we know that from Fresnel's equations we expect a loss of intensity according to $I_r/I_0 = 0.999017$ when passing through one RBC-layer surrounded by blood-plasma with $n_{ba}' = 1.345$. Thus, 16 sections will then cause a loss $I_r/I_0 = 0.999017^{16} = 0.984387$ due to a one-time backward reflection. In this work we only consider the forward transmitted wave and the one-time backward reflected wave in the Bremmer series and this is due to that the one-time reflected wave is very small. At the same time we also need to account for loss due to the absorption and as we have seen before the absorption coefficient is $\mu_a = 0.24mm^{-1}$. The total layer thickness having refractive index n_{rbc}' is $\Delta z = 16 \cdot 7.76\mu m = 124.16 \cdot 10^{-3}mm$ and thus, the intensity loss due to absorption will then theoretically become $I_a/I_0 = e^{-\mu_a \Delta z} = 0.970641$. In total, from theory, $I_{tot}/I_0 = 0.955029$. Turning to the computer simulation, using a discretization of $1024x1024$ in xy plane, which gives a discretized wavelength $\lambda = 632.8nm \longleftrightarrow 10.438$ nodes give $I_{tot}/I_0 = 0.945386$. Thus, a discripancy of 0.96%. Thus, from these results we can conclude that the implementation of the Bremmer series give a correct result which is important information before having more complicated geometries which in detail are impossible to verify theoretically.

3. The geometrical model

The geometrical model is a three-dimensional model describing the inhomogenous medium containing the blood plasma with imbedded RBCs. The number of RBCs within the model is denoted as N_{rbc}^3 and with N as the number describing the size of the mesh the size of the model will increase as N^3. It's easy to understand that the size of the model quite fast becomes very large and thus consuming a lot of RAM when increasing N. An estimate can be according to the following. Assume that we would like to have a model with $N_{rbc}^3 = 8^3 = 512$ number of RBCs, thus the plane wave propagating through the model will first encounter $8^2 = 64$ number of RBCs in a first layer, followed by another layer until we have reached 8 layers of RBCs in propagation direction z. We know that to be able to sample the wavelength at least 10 times and furthermore since the RBCs are rougly 10 times as large as the wavelength we need to describe the RBCs with roughly 100 nodes in one direction. It's conviniently set to $128 = 2^7$ for computational efficiency. This means, to be able to have enough resolution to compute the electric field over the entire model we need $N = 1024$ and thus the amount of RAM needed is then $1024^3 \cdot sizeof(double) \simeq 8.6 \cdot 10^9 = 8.6GB$ (assuming 64 bit double for describing the electric field in one point (z, y, x)). This is the reality if using the finite element method in a three-dimensional model and even if we would be able to make some clever meshing around the RBCs we would still need to be able to resolve the field in all points. Since the Bremmer series is an iterative approach we only need to keep $2N^2$ values in RAM at the same time. This applies for both the electric field and the geometrical model. The computer program written is only limited upon fundamental datatypes such as the size of an *int* and can thus in theory calculate models not even close to possible with other methods.

3.1. Brief model description

The programming of the model contain essentially two steps, the first is the initialisation step done during start of the simulation and in case of $N_{rbc} = 8$ it will create a three-dimensional model with 8^3 RBCs containing coordinates for the centers of all RBCs, it will also contain three Euler angles θ, ϕ, ψ which can be either set to a certain value or chosen to be random. Then each point will also contain a random translation in x and y up to the size of half an RBC. The random displacement is the same for all y coordinates in one $8x8$ layer of RBCs while for the same layer every $8x1$ row in x direction is translated independently of it's neighboor rows. Thus, translate the whole layer with $y + dy$ and then for a fix y every row with $x + dx$. This will make it possible to create an apparent randomness for the whole model. The requirement is that each RBC must not interfer with another RBC and to make this happen an RBC can rotate freely within a square box with the size of the maximum RBC size. This will put a constraint upon the hematocrit level, the volume-fraction can never be larger than the volume of the RBC in comparison to the quadratic box it resides within. While the first step was about creating a three-dimensional model at

Figure 3: Generated geometrical model of one layer RBC with random oriented Euler angles. Plotted by viewer3D MATLAB script. Notice the periodic boundary conditions.

RBC-level the second step is about meshing up a two-dimensional layer with N^2 nodes containing a representation of either an RBC or blood plasma.

3.2. Describing the RBC

Calculating the electric field in a point (y, x) belonging to the layer z_n requires us to find an expression $f(z_n, y, x) = 0$ for the boundary of the RBC since we need to know the permitivity ϵ_r to use. And the expression shall be such that if $f(z_n, y, x) \leq 0$ the point (y, x) is within the RBC, otherwise outside. Thus, we can create a two-dimensional matrix $slow[y][x]$ containing the value 1 if within RBC and 0 if not. During the calculation of the field we can then use $slow[y][x]$ to convert the ones and zeros to represent the relative permitivity, if $slow[y][x] = 1$ then $\epsilon_r = \epsilon_{rbc}$ and if $slow[y][x] = 0$ then $\epsilon_r = \epsilon_{plasma}$ (real-parts in this context). During calculations also the relative permitivity between blood plasma and RBC is used, thus the RBC is assigned the permitivty $\epsilon_{rbc}/\epsilon_{plasma}$. To be able to determine whether a coordinate is within or outside an RBC a parametric model is used describing the boundary of the RBC e.g. [17]

$$D(z_n)^2 = 4 \cdot z_n^2 - (1 - (\frac{R}{R_0})^2 \cdot (C_0 + C_2(\frac{R}{R_0})^2 + C_4(\frac{R}{R_0})^4)^2 \qquad (29)$$

where $R = x^2 + y^2$. If $(y, x) \rightarrow D(z_n)^2 \leq 0$ the coordinate (y, x) is within the RBC and can be marked as "1". The constants describe the cell-shape and are chosen according to [17] and then re-calculated into nodes.

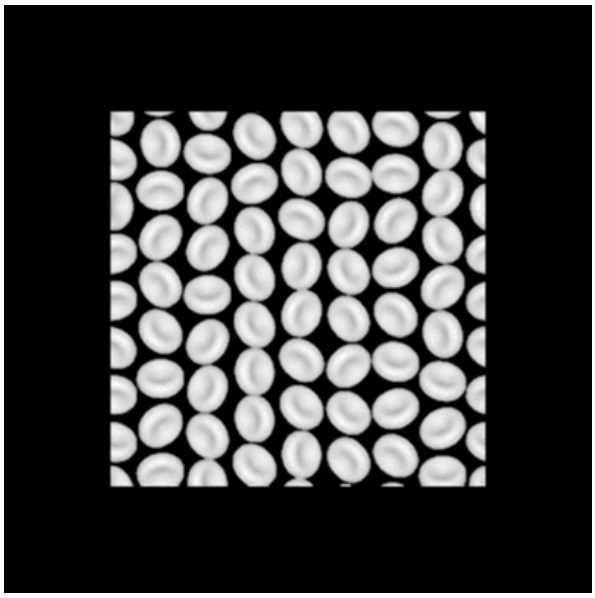

Figure 4: Generated geometrical model with Euler angle $\theta = \pi/4$ and otherwise random orientation. Plotted by viewer3D MATLAB script.

We have mentioned that the model is of size N^3 but we are not limited to N in propagation direction. After calculating the electric field for the N^3 problem we can start over from the beginning again by creating a new N^3 model and use the electric field from the first model as initial value. And so further. The idea is so simple but yet so brilliant and enables an in theory infinite simulation in propagation direction. The caveat is of course that the field must not have a too much of it's power scattered in the xy plane. Simulations indicate that this is not the case and thus the method should work fine. Figures 3 and 4 shows the output from the simulation where one layer of RBCs are displayed for two different setup of the Euler angles. We also see the effect of the random-translation in x and y direction performed so that we get periodic boundary conditions.

3.3. Euler angels and translation

Since we have created a model with centers in a global coordinate system we need to be able to transform this coordinate system into a local coordinate system where an RBC can be described. In the previous section we described a parametric expression for the RBC which is valid in a coordinate system with symmetry around the axle through a center of the RBC. However, in our three-dimensional model the RBC have coordinates in a global coordinate system and furthermore we have chosen to have random displacement as well as describing the orientation of the RBC with Euler angles. Thus, we need to transform the global coordinates into a local coordinate system which is rotated. Furthermore

we know that translation and rotation of a cartesian coordinate system does not cause any scaling of distances. Let (z_c, y_c, x_c) be the coordinates for the center of an RBC in a global coordinate system. A point (z, y, x) can the be described in a local coordinate system of the RBC as (z_l, y_l, x_l)= (z, y, x)- (z_c, y_c, x_c). In the local coordinate system the RBC is rotated with Euler angels θ, ϕ, ψ and to tranform (z_l, y_l, x_l) into a rotated coordinate system (z_e, y_e, x_e) we use $\bar{x_e} = A \cdot \bar{x}_l$ where A is the matrix (see e.g. [32])

$$A = \begin{bmatrix} a_{11} & a_{12} & a13 \\ a_{21} & a_{22} & a_{23} \\ a_{31} & a_{32} & a_{33} \end{bmatrix}$$

$$\begin{aligned} a_{11} &= cos(\psi)cos(\phi) - cos(\theta)sin(\phi)sin(\psi) \\ a_{12} &= cos(\psi)sin(\phi) + cos(\theta)cos(\phi)sin(\psi) \\ a_{13} &= sin(\psi)sin(\theta) \\ a_{21} &= cos(\psi)sin(\phi) + cos(\theta)cos(\phi)sin(\psi) \\ a_{22} &= -sin(\psi)sin(\phi) + cos(\theta)cos(\phi)cos(\psi) \\ a_{23} &= -sin(\theta)cos(\phi) \\ a_{31} &= sin(\theta)sin(\psi) \\ a_{32} &= sin(\theta)cos(\psi) \\ a_{33} &= cos(\theta) \end{aligned}$$

Thus $\bar{x_e} = A \cdot [(z, y, x) - (z_c, y_c, x_c)]$. Using this transformation makes it possible to determine whether a point in the global coordinate system is within or outside an RBC having it's center in (z_c, y_c, x_c).

4. Results

4.1. Single RBC scattering

In this section we will look at the result from the Bremmer series when considering scattering from a single RBC. This has been done in [17] [25] using finite-difference time-domain method (FDTD), Rytov approximation and the discrete dipole approximation (DDA). The idea in this article is to be able to compare the far-field with these results as well as to understand how the electric field evolves within the RBC for different orientations, e.g. $\theta = 0$ and $\theta = \pi/2$. When investigating a whole model containing several hundreds of thousands of RBCs, possibly randomly distributed it can be hard to understand the effect from the scattering of individual RBCs. However, these simulations are important to find possible patterns depending upon orientation of the RBCs both by studying the field in the xy plane as well as zx and zy plane. Since it's hard to graphically handle a three-dimensional model we instead make vertical and horizontal cuts to display the field in two-dimensional planes within the model. This will give us a fair understanding of how the field interacts with and within the RBCs.

4.1.1. The electric near-field

The results from the calculation of the near-field can be seen Figure 5-17.

To be able to better understand the dynamics of the propagation the following URL can be used to see behavior for an RBC oriented with $\theta = 0$.

`https://1drv.ms/v/s!Ar_QTSP_vqJPhPc8VJB-goLTv7hQIg?e=78oL58`

We can see the absolute value of the electric field in the xy plane while the wave is propagating in the z direction and passing through the RBC. The simulation is generated between $z_n = 350 \rightarrow 750$ (see Figures 5-7) . From the simulation we can see that when the wave has propagated through half of the RBC the electric field is building up strongly along the edges of the RBC. When the wave is leaving the RBC there is one main-ray and two strong rays on both sides. We also see that the main-ray weakens in what could be interpreted as the focal-point of the RBC. Thus, the RBC act as a convex lens focusing the light. In this paper we are only dealing with a scalar field but even though it can be showed that if taking the polarization into account the from beginning zero-components will cancel out in the focal point. Thus, if having an inital wave $\bar{E} = \hat{x} \cdot E_0 Re(e^{j(\omega t - kz)})$ then during propagation both $\hat{x}$ and $\hat{y}$ components will appear due to boundary conditions each with strength described by Fresnel equations. At the focal point though the $\hat{y}$ component will cancel out. This has been discussed in [33] where it's also analytically derived for the case of a sphere.

In analogy to the case of $\theta = 0$ a dynamic simulation for $\theta = \pi/2$ can be viewed in the following link

`https://1drv.ms/v/s!Ar_QTSP_vqJPhPc9D3OacT4eQZtcaw?e=yEcjb0`

The wave as in the previous case show the absolute value of the electric field. The simulation is as previously generated between $z_n = 350 \rightarrow 750$. What we can see from this simulation is that initially the strength of the field is evenly increased when starting to interact with the RBC after roughly 2 seconds. After roughly 5 seconds the field starts to increase along the edges immidiately after the first maximum of the RBC thickness. The field then increases even further and it spreads to the center of the disk where it is being squeezed between the surfaces until the middle of the disk has been reached. This is where the distance between RBC surfaces has it's minimum. The field stays high along the edges while the center oscillates between high and low field-strength. When having passed through the RBC the light then leaves the disk in one main-ray forward and two rays at each side which can also be seen in Figure 5-6. As for the case $\theta = 0$ we can see how the RBC focuses the ligth. This is also described in [33] where they connect to a larger area being exposed to a larger energy focused at the central line. What is clear though is that the more the field interact with the RBC, the more energy is focused. The distance to the focal-point is is shorter for $\theta = 0$ which probably can be explained by the difference in curvature between the two orientations.

4.1.2. Far field calculation

The far-field calculation is done to be able to compare the results from the Bremmer series approach with other studies using e.g. FDTD and DDA. A usually used limit between near-field and far-field is the Frauenhofer distance

$$d_F = 2D^2/\lambda \tag{30}$$

where D is the typical object size and λ the wavelength. In our case this would roughly mean $d_F \simeq 2 \cdot 7.76^2/0.6328 = 190\mu m$. Thus, if the RBC is sampled with 128 nodes we would need $n = 128 \cdot 190/7.76 \simeq 3140$ nodes in propagation direction. And this would also imply very narrow scattering angle unless we create a huge model which is not possible in the context of this study where all calculations are done with a laptop within an hour or two for a 1024^3 model. Thus we need to have a way to transform the near-field into a far-field by other means.

4.2. Scattering from multiple RBCs

For the multiple scattering case a simulation can be seen at

`https://1drv.ms/v/s!Ar_QTSP_vqJPhPc_mJKmivLwgJ-yZw?e=jr6nWv`

where the wave is scattered against $8x8x8$ RBCs with random orientation in a $1024x1024x1024$ model where calculation time is approximately $1.5hours$. What can be seen is that initially waves in transeverse direction is created for each of the objects and interference occurs between the waves. As for the case with only one RBC we can see the increase of intenstity along the edges of the RBC where the light gets trapped. Quite soon the wave-motion stops and left is a fluctuating speckle pattern. In Figure 17-21 we can also see a vertical cut of the field.for a model having $4x4x4$ RBCs.

4.3. Full scattering

Q1: Does the orientation of first layer play any major roll? What is the difference if first layer is pi half or 0 and the rest is random? Plot this, all random, first pi half and then first 0.

Q2: Simulate field with 2048x2048 and 16x16 RBC in xy. Plot cut in z-direction and xy field. Gives overview of behaviour.

4.4. Intensity variation

Simulation of field.

4.5. Appendix

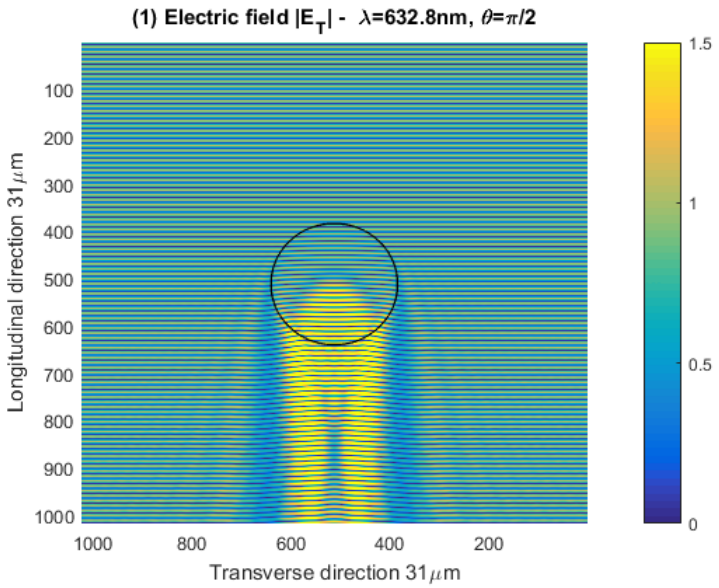

Figure 5: Near-field scattering of one RBC with $\theta = \pi/2$

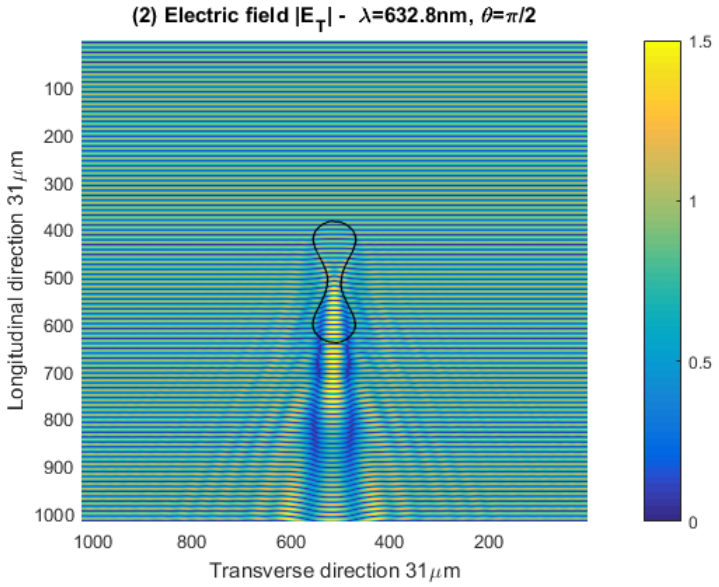

Figure 6: Near-field scattering of one RBC with $\theta = \pi/2$

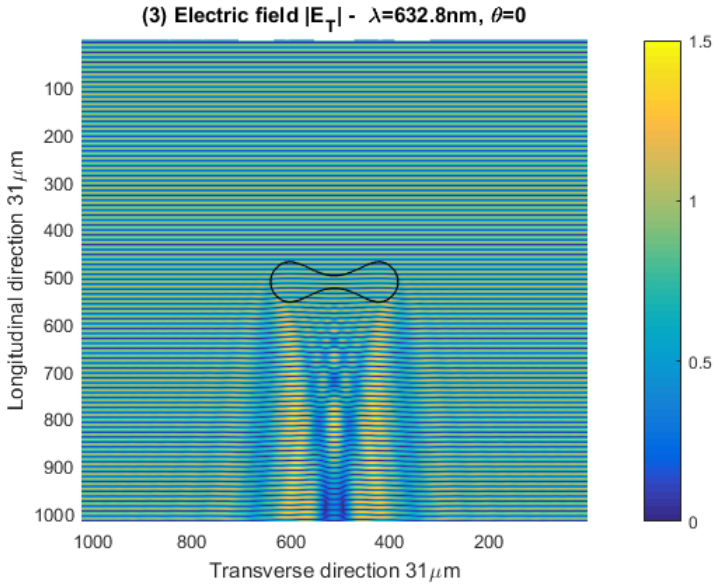

Figure 7: Near-field scattering of one RBC with $\theta = 0$

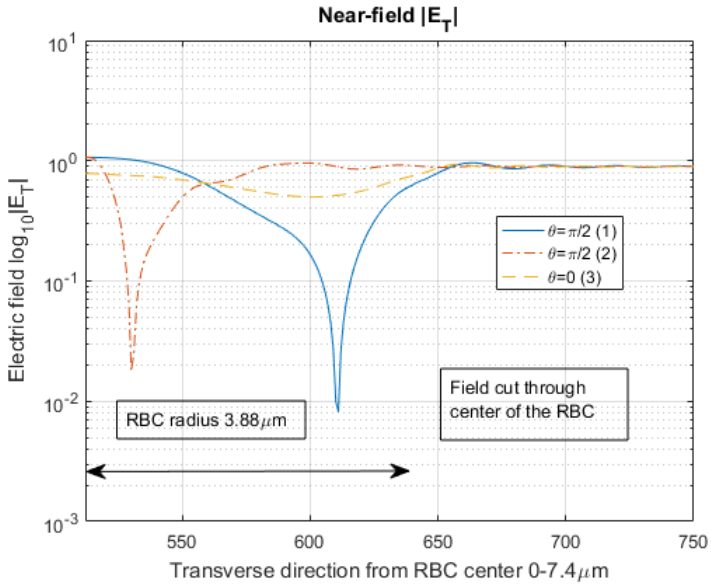

Figure 8: The electric near-field from xy plane cut through the center ($z_n = 512$) of the RBC.

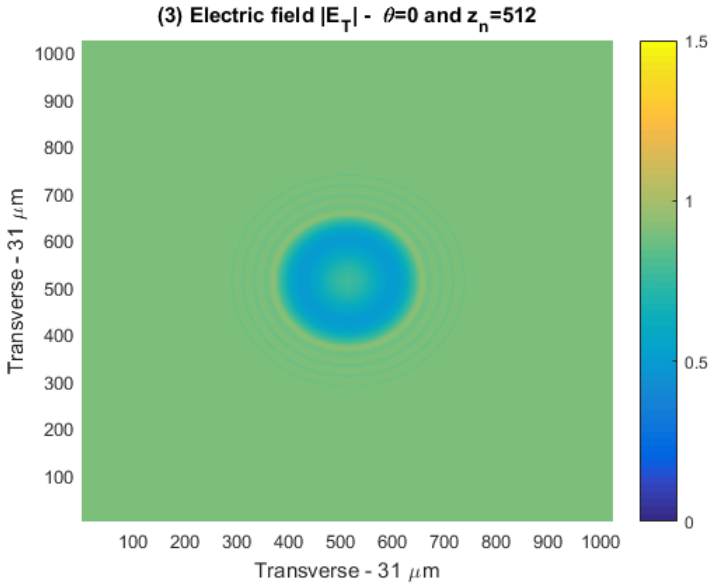

Figure 9: Electric field in xy plane at $z_n = 512$.

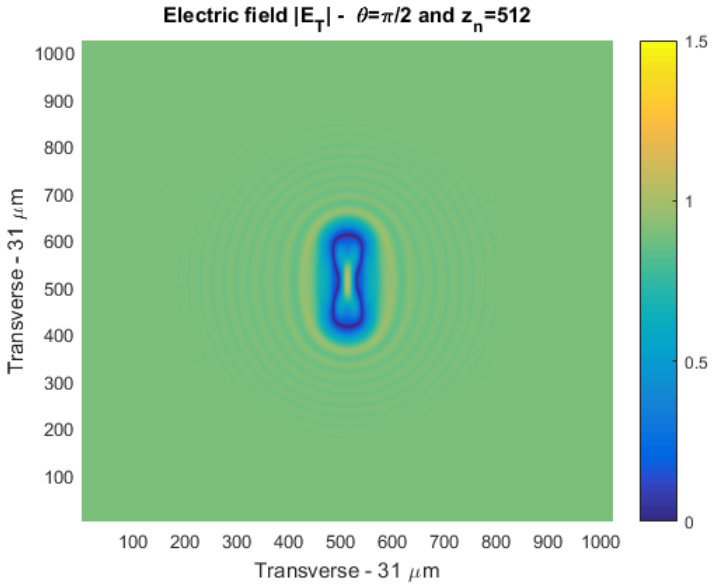

Figure 10: Electric field in xy plane at $z_n = 512$

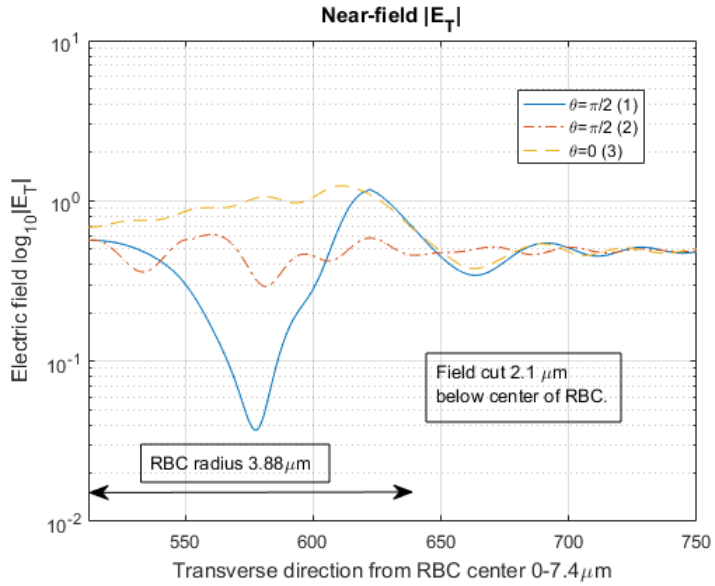

Figure 11: The electric near-field from xy plane cut $2.1\mu m$ below center ($z_n = 580$) of the RBC.

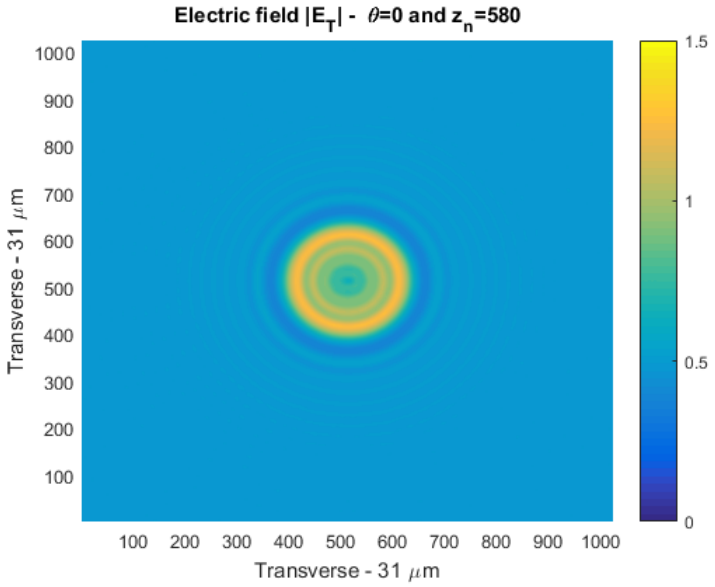

Figure 12: Electric field in xy plane at $z_n = 580$.

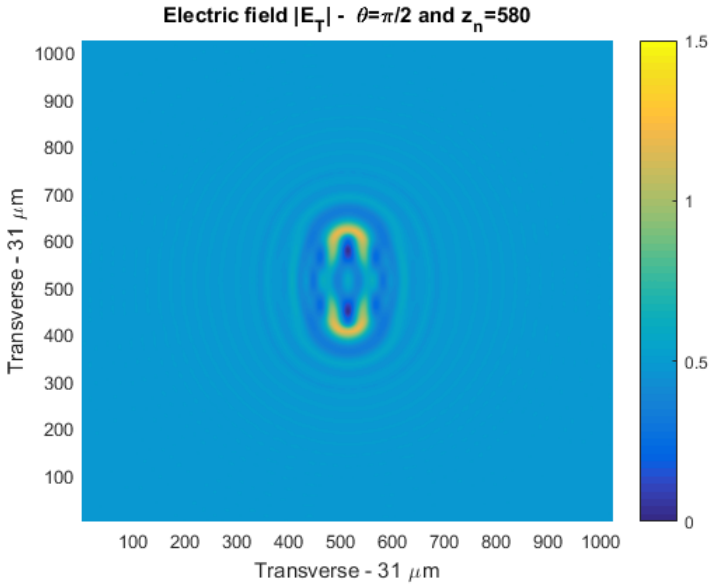

Figure 13: Electric field in xy plane at $z_n = 580$.

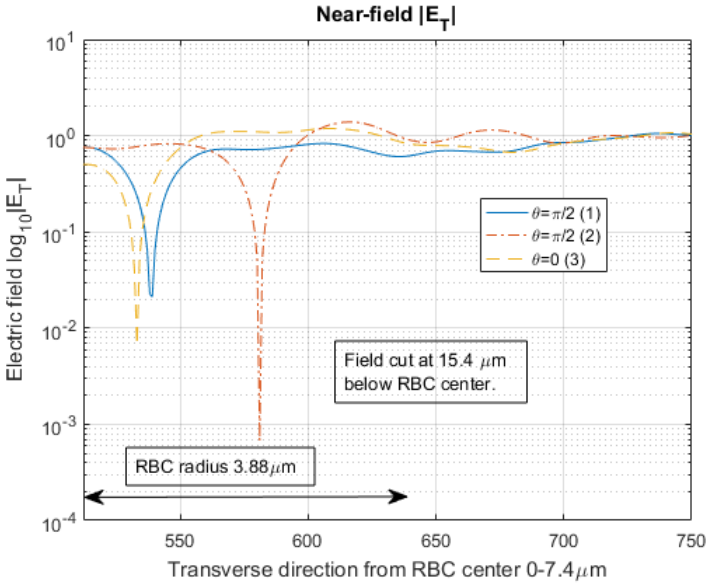

Figure 14: The electric near-field from xy plane cut $15.4\mu m$ below center ($z_n = 1021$) of the RBC

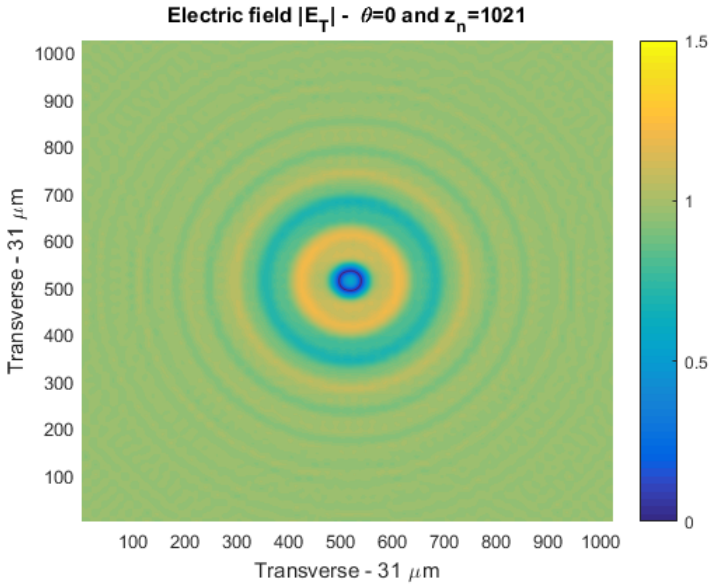

Figure 15: Electric field in xy plane at $z_n = 1021$

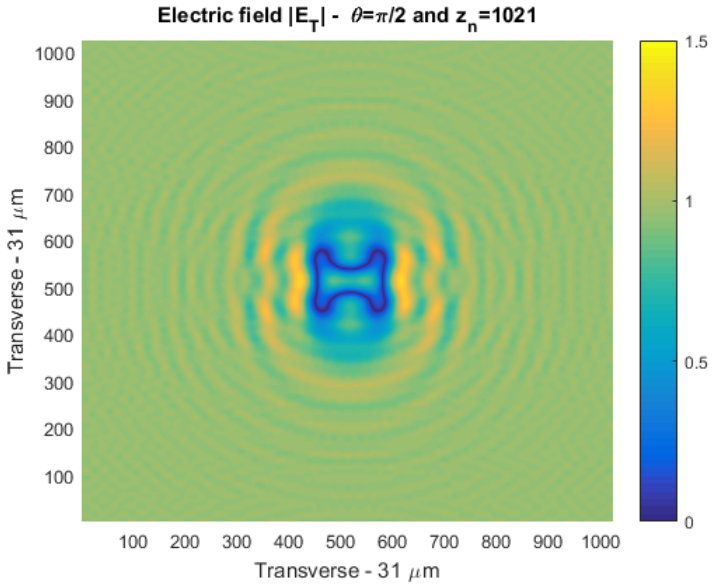

Figure 16: Electric field in xy plane at $z_n = 1021$

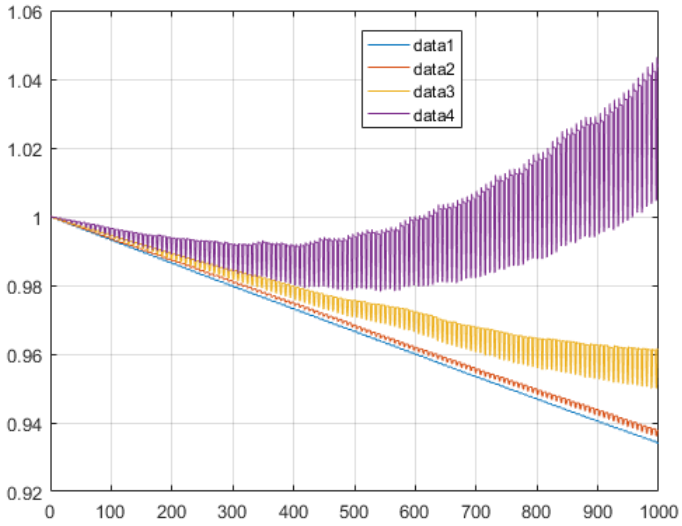

Figure 17: Intensity variation for different contrasts between RBC and background.

References

[1] Akira Ishimaru, Electrmagnetic Wave Propagation, Radiation, and Scattering, Wiley (2017)

[2] Nienke Bosschaart, A literature review and novel theoretical approach on the optical properties of whole blood

[3] S. A. Prahl, A Monte Carlo Model of Light Propagation in Tissue, SPIE Institute Series Vol. IS 5 (1989)

[4] A. G. Borovoi, Scattering of light by a red blood cell, Journal of biomedical optics (1998)

[5] Scott burdick, One-way wave propagators for velocity analysis on curvilinear coordinates, Massachusetts Institute of Technology

[6] D. Chicea, Computer simulation results of light scattered on red blood cells, Physics Department, University Lucian Blaga

[7] H.L. Berk, Convergence of the bremmer series for the spatially inhomogeneous helmholtz equation, Trieste June (1966)

[8] Hamootal Duadi, Dependence of light scattering profile in tissue on blood vessel diameter and distribution: a computer simulation study, Journal of Biomedical Optics (2013)

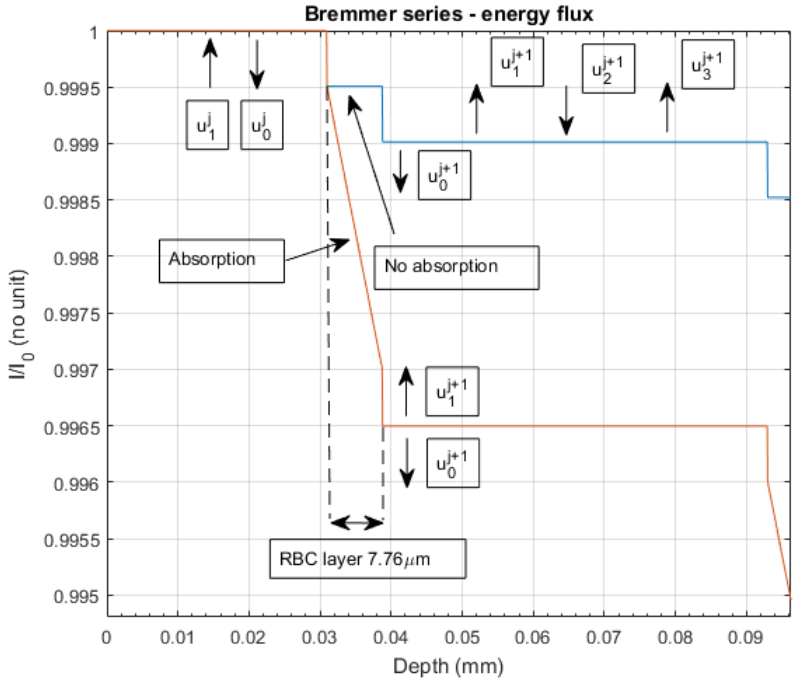

Figure 18: The one-dimensional slab

[9] Maxim A. Yurkin, Experimental and theoretical study of light scattering by individual mature red blood cells by use of scanning flow cytometry and discrete dipole approximation

[10] Chris H. Chapman, Fundamentals of seismic wave propagation, Cambridge University Press (2004)

[11] Mattheus J.N. Van Stralen, Generalized Bremmer series with rational approximation for the scattering of waves in inhomogeneous media (1998)

[12] Eugene Hecht, Optics, Addision-Wesley (1987)

[13] G. Milton Wing, Invariant Imbedding and Generalizations of the WKB Method and the Bremmer Series, Journal of mathematical analysis and applications (1974)

[14] Michael I. Mishchenko, Light Scattering by Nonspherical Particles Theory, Measurements, and Applications, Academic Press (2000)

[15] Thomas Wriedt, Light scattering theories and computer codes, Journal of Quantitative Spectroscopy and Radiative Transfer (2009)

[16] Wesley B. Baker, Modified Beer-Lambert law for blood flow, Optical Society of America (2014)

[17] Karlsson, Anders, Numerical simulations of light scattering by red blood cells, Lund University (2005)

[18] D. Yim, On the Modeling of Light Interactions with Human Blood, University of Waterloo (2011)

[19] Richard Bellman, On the principle of invariant imbedding and propagation through inhomogeneous media, Rand Corporation, Santa Monica, California (1956)

[20] Sophocles J. Orfanidis, Electromagnetic Waves and Antennas, Rutgers University (2016)

[21] Philip W. Kuchel, Parametric-Equation Representation of Biconcave Erythrocytes, Bulletin of Mathematical Biology (1999)

[22] Shuang Chang, Review of methods and applications of attenuation coefficient measurements with optical coherence tomography, Journal of Biomedical Optics (2019)

[23] Bjoern Ursin, Seismic migration using the WKB approximation, Geophys. J. R. astr. Soc. (1984)

[24] M V Berry, Semiclassical approximations in wave mechanics, Rep. Prog. Phys. (1972)

[25] Jun Q. Lu, Simulations of light scattering from a biconcave red blood cell using the finite-difference time-domain method, Journal of Biomedical Optics (2005)

[26] Gustafsson, Mats, The Bremmer series for a multi-dimensional acoustic scattering problem, Lund University (2005)

[27] Nilsson, Annika, T-matrix computations of light scattering by red blood cells, Lund University (1998)

[28] F.V. Atkinson , Wave Propagation and the Bremmer Series, Journal of mathematical analysis and applications (1960)

[29] Gustafsson, Mats, Wave Splitting in Direct and Inverse Scattering Problems, Lund University (2000)

[30] R. Bellman, Wave Equation with Sources, Invariant Imbedding, and Bremmer Series Solutions, Journal of mathematical analysis and applications (1974)

[31] F.V. Atkinson, Wave Propagation and the Bremmer Series, Journal of mathematical analysis and applications (1960)

[32] Herbert Goldstein, Classical mechanics, Addison-Wesley (1980)

[33] Jornet, Josep Miquel, Nanoscale Optical Wireless Channel Model for Intra-Body Communications: Geometrical, Time and Frequency Domain Analysis, IEEE Transactions on Communications (2018)

[34] Lennart Råde, BETA Mathematics Handbook, Studentlitteratur